Spatial and temporal variation of $\delta^{13}C$ values of methane emitted from a temperate mire: Methanogenesis, methanotrophy, and hysteresis

Janne Rinne[1,2], Patryk Łakomiec[1], Patrik Vestin[1], Joel D. White[1], Per Weslien[3] Julia Kelly[4], Natascha Kljun[4], Lena Ström[1], Leif Klemedtsson[3]

[1]Lund University, Department of Physical Geography and Ecosystem Science, Lund, Sweden
[2]Natural Resources Institute Finland, Production Systems Unit, Helsinki, Finland
[3]University of Gothenburg, Department of Earth Sciences, Gothenburg, Sweden
[4]Lund University, Centre for Environmental and Climate Science, Lund, Sweden

Correspondence to: Janne Rinne (janne.rinne@luke.fi)

Abstract. The reasons for spatial and temporal variation of methane emission from mire ecosystems are not fully understood. Stable isotope signatures of the emitted methane can offer clues to the causes of these variations. We measured the methane emission (F_{CH4}) and ^{13}C-signature ($\delta^{13}C$) of emitted methane by automated chambers at a temperate mire for two growing seasons. In addition, we used ambient methane mixing ratios and $\delta^{13}C$ to calculate a mire-scale ^{13}C signature using a nocturnal boundary-layer accumulation approach. Microbial methanogenic and methanotrophic communities were determined by a captured metagenomics analysis. The chamber measurements showed large and systematic spatial variations in $\delta^{13}C$-CH_4 of up to 15 ‰ but smaller and less systematic temporal variation. According to the spatial $\delta^{13}C$-F_{CH4} relations, methanotrophy was unlikely to be the dominating cause for the spatial variation. Instead, these was indication for the substrate availability of methanogenesis to be a major factor explaining the spatial variation. Genetic analysis indicated that methanogenic communities at all sample locations were able to utilize both hydrogenotrophic and acetoclastic pathways and could thus adapt to changes in the available substrate. The temporal variation of F_{CH4} and $\delta^{13}C$ over the growing seasons showed hysteresis-like behavior at high-emission locations, indicative of time-lagged responses to temperature and substrate availability. The up-scaled chamber measurements and nocturnal boundary-layer accumulation measurements showed similar average $\delta^{13}C$ values of -81.3 ‰ and -79.3 ‰, respectively, indicative of hydrogenotrophic methanogenesis at the mire. The close correspondence of the $\delta^{13}C$ values obtained by the two methods lend confidence to the obtained mire scale isotopic signature. This and other recently published data on $\delta^{13}C$ values of CH_4 emitted from northern mires are considerably lower than the values used in atmospheric inversion studies on methane sources, suggesting a need for revision of the model input.

1 Introduction

Methane (CH_4) is the one of the three main drivers of anthropogenic climate change. Its sources include both biological and anthropogenic processes, with the most significant natural source being wetland ecosystems (Ciais et al., 2013). As changing climate may influence global CH_4 emission from wetlands, a mechanistic understanding of the processes behind these emissions is crucial.

The CH_4 emission rates from wetlands are controlled by CH_4 production (methanogenesis), CH_4 oxidation (methanotrophy), and the transport of CH_4 from peat into the atmosphere (e.g. Lai, 2009). A fundamental factor for CH_4 production by Archaea is the availability of substrates, as H_2 or acetate for hydrogenotrophic or acetoclastic methanogenesis, respectively (e.g. Lai, 2009). Furthermore, temperature is a key driver of the CH_4 emission rate via its effect on microbial activity, as seen by the incubations of peat samples conducted at different temperatures (Juottonen at al., 2008). Water table position and the presence of alternative electron acceptors can also influence the spatial or temporal behavior of CH_4 production (e.g. Serrano-Silva et al., 2014). A part of the produced CH_4 is commonly oxidized in the wetland, and thus not emitted into the atmosphere (e.g. Larmola et al., 2010). This methanotrophy is caused by methanotrophic micro-organisms (bacteria), and it may also be dependent on temperature (Serrano-Silva et a., 2014). Finally, CH_4 can be transported from the anoxic layers to the atmosphere by three different mechanisms: diffusion through the peat matrix, ebullition, and plant mediated transport (Lai, 2009). The later can be further divided into passive diffusive transport and active convective transport (Brix et al., 1992).

The observed CH_4 emissions from wetland ecosystems exhibit both temporal and spatial variations, which reflect the variation in the above-mentioned processes, often in tandem. Typically, CH_4 emission rates vary spatially over short distances following surface microtopography (e.g. Riutta et al., 2007; Keane et al., 2021), and related differences in vegetation characteristics. The highest emission rates are commonly observed in wetter locations, with abundant aerenchymatous vegetation, whereas the lowest emission rates are observed at dry hummocks or inundated locations (e.g. Riutta et al., 2007, Keane et al., 2021). This microtopography-scale spatial variation in CH_4 emission can be caused by differences in the methanogenesis, methanotrophy, or transport pathways in these different locations (Joabsson et al., 1999; Joabsson & Christensen 2001).

Temporally, we commonly see a seasonal cycle in the CH_4 emission rates, with the highest emission rates in late summer (Rinne et al., 2018; Heiskanen et al., 2021b; Łakomiec et al., 2021). This seasonal variation has been associated with the seasonal cycle of peat temperature, substrate availability, and transport pathways (Rinne et al., 2018; Chang et al., 2020; 2021). Diel variation of CH_4 emission rates has also been observed in wetlands with vegetation such as *Phragmites*, *Typha*, and *Nymphaea* that exhibits pressurized airflow into the root systems, (Kim et al., 1998; Kowalska et al., 2013), whereas

wetlands with vegetation that exhibits diffusive air transport show little or no diel cycle in their CH_4 emission (Rinne et al., 2007; Jackowicz-Korczyński et al., 2010; Kowalska et al., 2013). In many cases the predominance of any one cause for temporal variation in CH_4 emission may be difficult to verify, as the variation of these different processes may lead to similar variations in the resulting CH_4 emission rate (Chang et al., 2021).

CH_4 emitted from different sources (e.g. wetlands with different methanogenic pathways, waste, ruminants, termites etc.) is characterized by different isotopic composition (Miller, 2005; Hornibrook 2009), and this isotopic composition can offer clues to the processes behind these emissions. The major component of CH_4, carbon, has two stable isotopes, ^{12}C and ^{13}C, which make up 98.9% and 1.1% of carbon in nature, respectively. While different isotopes of the same element behave chemically identically, their different masses cause differences in their diffusion rates, and in the rates of many chemical and biological processes. This will lead to differences in the isotopic ratios of CH_4 as it goes through methanotrophy, methanogenesis or transport from the anoxic peat layers to the atmosphere

In mire ecosystems, which are defined as vegetated wetlands with capability for peat formation (Lindsay 2018), the ^{13}C signature, or $\delta^{13}C$ value, of emitted CH_4 depends on its production pathway, and subsequent transport and oxidation (Hornibrook, 2009). Of the two dominating methanogenic pathways in wetlands, hydrogenotrophic methanogenesis typically produces CH_4 that has lower $\delta^{13}C$ value than CH_4 produced by acetoclastic pathway (Hornibrook, 2009). Furthermore, microbial oxidation of CH_4 can shift the emitted CH_4 to have higher $\delta^{13}C$ value, as microbial methanotrophy prefers ^{12}C-CH_4 (Hornibrook 2009). Thus, the $\delta^{13}C$ values of the emitted CH_4 can be used as an additional constraint when interpreting the observed CH_4 emission rates to disentangle the processes responsible for the spatial and temporal variation in CH_4 emission. For example, recent analysis has shown hysteresis-like behavior between surface temperatures and CH_4 emission rates in mire ecosystems, and the possible causes of this phenomenon are debated (Chang et al., 2020; 2021; Łakomiec et al., 2021). Similar hysteresis-like behavior has also been observed between photosynthesis and CH_4 emission rates (Rinne et al., 2018). Stable isotope signatures of emitted methane can constrain our hypotheses on the causes of these behavior by refutation or corroboration.

In this study, we analyze the observed spatial and temporal variation of CH_4 emission rates from a temperate mire ecosystem and its $\delta^{13}C$ values to understand the causes of these variations. We aim to shed light on the relative importance of methanogenesis and methanotrophy for the spatial variation in the CH_4 emission rate, and the roles of precursor substrate availability and temperature for the seasonal variation of the CH_4 emission rate. We also use taxonomy data to characterize the methanogenic and methanotrophic microbial communities in the mire to reveal the potential of methane production via different pathways as well as microbial methane oxidation.

In order to interpret the variation in CH_4 emission rates and their $\delta^{13}C$ values, we have formulated a conceptual framework with different simplified hypotheses for the causes of the spatial and temporal variations of methane emission rates. From these we have deduced expected relations between CH_4 emission rates and their $\delta^{13}C$ values, that are used to guide the data analysis and interpretation.

2 Conceptual framework

We will consider two commonly observed phenomena in the variation of CH_4 emission rates from mires. First, there is a spatial variation at the microtopographic level, with the lowest emissions from dry hummocks and inundated ponds and highest emissions from wet lawns (e.g. Riutta et al., 2007; Keane et al., 2021). Second, there is a temporal variation at the seasonal scale, which lags the cycle of air and peat surface temperature and GPP, but follows the temperature of deeper peat (e.g. Rinne et al., 2018; Chang et al., 2020; 2021; Łakomiec et al., 2021).

We can have two simplified hypotheses regarding the processes leading to the small-scale spatial variability of the CH_4 emission rate. In the first hypothesis on spatial variability (HS1), we assume that the production of CH_4 beneath wetter and drier surfaces is equal but that oxidation by methanotrophic organisms in the oxic layers leads to lower emission of CH_4 from the drier surfaces compared to the wetter surfaces (Figure 1). In the second spatial hypotheses (HS2), we assume that the differences in CH_4 emission rate between wet and dry surfaces reflect differences in CH_4 production due to differences in the substrate availability for methanogenesis. While both hypotheses lead to similar differences in the CH_4 emission rates between the wetter and drier surfaces, their relation to the $\delta^{13}C$ values are different. HS1 would lead to negative correlation between CH_4 emission rate and $\delta^{13}C$ value of emitted CH_4, because enzymatic reactions associated with methanotroph metabolism consumes preferentially $^{12}CH_4$, resulting ^{13}C enrichment of residual CH_4. HS2, on the other hand, would lead to positive correlation between CH_4 emission rate and its $\delta^{13}C$ value, because CH_4 production in conditions with better substrate availability, typically associated with higher methane emission rates of more productive mires, leads to CH_4 with higher $\delta^{13}C$ value than in lower substrate availability (Chanton et al., 2005). The better substrate availability can be associated with acetate availability for acetoclastic methanogenesis or better energetics for hydrogenotrophic methanogenesis (Penning et al., 2005; Hornibrook 2009). Thus, the two hypotheses lead to distinctly different predictions on the relationship between CH_4 emission rate and its $\delta^{13}C$ value (Hornibrook 2009). As a zero hypothesis (HS0) we may have e.g. a mixture of the above mentioned processes contributing to the spatial variability of CH_4 emission. In this case we may observe no systematic co-variation between CH_4 emission rate and $\delta^{13}C$ values.

For the seasonal variation of CH_4 emission rate, we can hypothesize that the variation is either due to the seasonal development of temperature, or that it is modified heavily by the availability of substrates for methanogenesis (Chang et al.,

2020; 2021). In the first hypothesis on the temporal variation (HT1), we assume that the temporal variation is due to the seasonal change in peat temperature. As this does not change the $\delta^{13}C$ value of emitted CH_4, there will be no temporal correlation between CH_4 emission rate and its $\delta^{13}C$ value (Figure 2). In the second temporal hypothesis (HT2) we assume that the seasonal cycle of the CH_4 emission rate is due to the changes in substrate availability. This may be via changes in availability of H_2 for hydrogenotrophic methanogenesis or by availability of acetate for acetoclastic methanogenesis. Thus, the changes of substrate availability may or may not include changes in the methanogenetic pathway. The HT2 would lead to positive correlation between CH_4 emission rate and its $\delta^{13}C$ value. In the third temporal hypothesis (HT3) we assume that there are significant time lags between the seasonal cycles of the drivers of CH_4 emission rate, i.e. temperature and substrate availability, which leads to hysteresis-like behavior in the relationship between CH_4 emission rate and its $\delta^{13}C$ value.

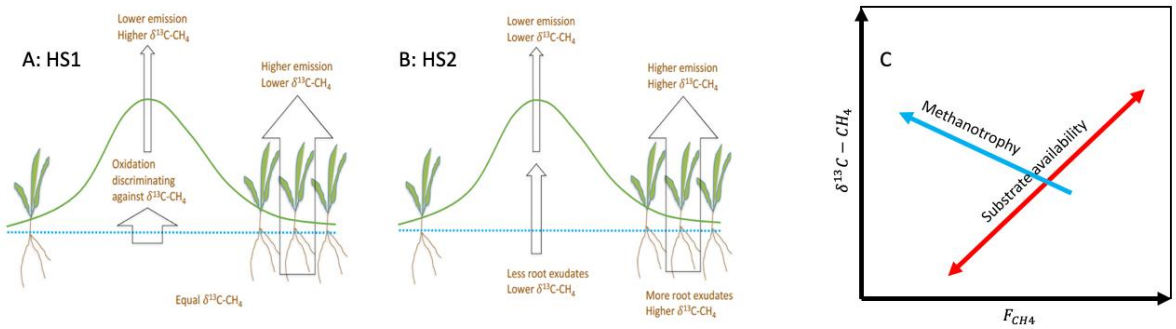

Figure 1: Spatial variation of methane emission based on two hypotheses: A: HS1, variation is due to methanotrophy; and B: HS2, variation is due to methanogenesis and substrate status. Resulting relations between $\delta^{13}C$-CH_4 and F_{CH4} are shown in panel C.

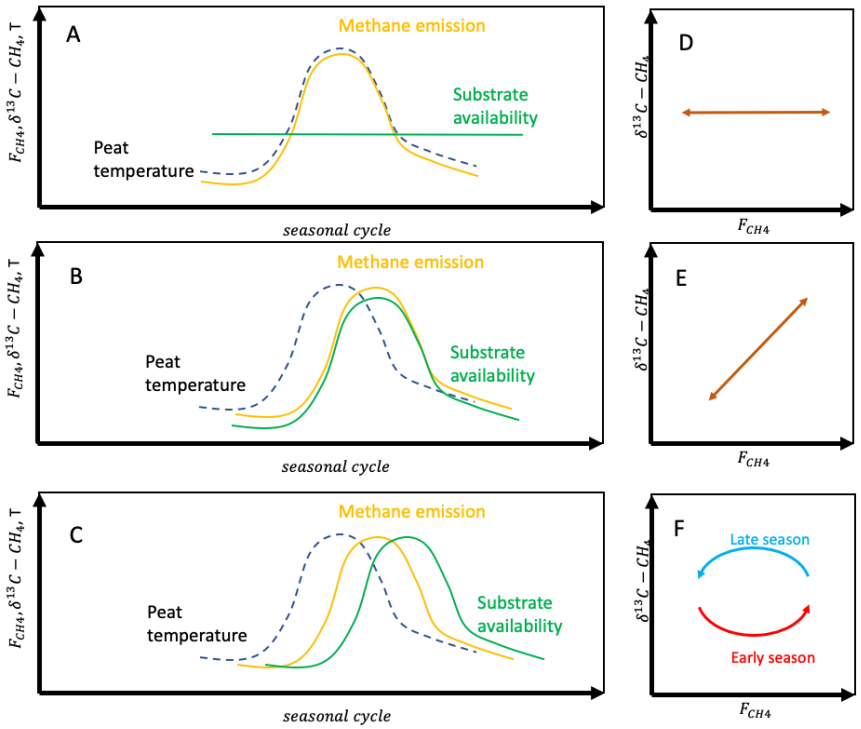

Figure 2: Seasonal variation of methane emission with hypotheses on controlling processes (A: HT1; B: HT2; C: HT3) and resulting relations between $\delta^{13}C$-CH_4 and F_{CH4} (D-F).

3 Methods

3.1 Study site and ancillary measurements

We conducted the measurements at Mycklemossen mire (58°21'N 12°10'E, 80 m a.s.l., Figure 3) in south-western Sweden in 2019 and 2020. The site is a part of SITES[1] Skogaryd research catchment and a candidate to be a class 2 ecosystem site within the ICOS[2] research infrastructure (Heiskanen et al., 2021a). Mycklemossen mire lies within the temperate / hemiboreal forest zone. The annual 30-year average air temperature from a nearby weather stations is 6.8°C (1981-2010, SMHI Vänersborg) and annual precipitation is 800-1000 mm (1981-2010, SHMI Vänersborg and Uddevalla). The mire is a poor fen with bog characteristics in its vegetation and pH of 3.9-4.0 (Rinne et al., 2020).

[1] Swedish Infrastructure for Ecosystem Science, https://www.fieldsites.se/
[2] Integrated Carbon Observation System, https://www.icos-cp.eu/

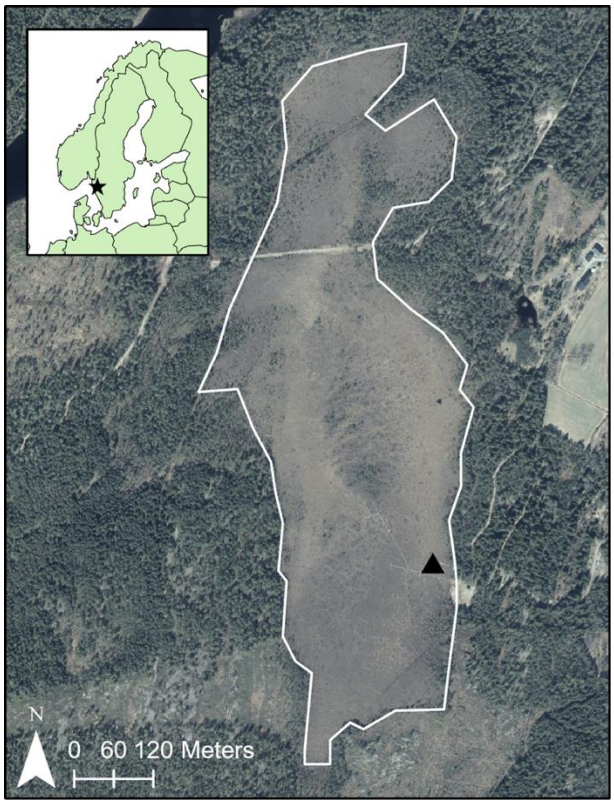

Figure 3: Map of Mycklemossen (outlined in white). Black star indicates the location of Mycklemossen within Scandinavia, black triangle indicates the location of the chamber and NBLA measurements. Data sources: © Lantmäteriet, © EuroGeographics.

A range of meteorological and hydrological parameters are available from the Mycklemossen research site, including air temperature, peat temperature at different depths at four locations, and water table position at three locations.

3.2 CH_4 emission and $\delta^{13}C$ measurements

We used two approaches to measure the $\delta^{13}C$ value of the emitted CH_4, the automated static chamber approach (e.g. McCalley et al., 2014) and the nocturnal boundary-layer accumulation (NBLA) approach (e.g. Sriskantharajah et al., 2012). With the former we obtain CH_4 emission rate and its $\delta^{13}C$ value resolved at the microtopographic scale, while with the latter we obtain an average $\delta^{13}C$ value of the emitted CH_4 over a larger area of the mire.

For the chamber approach, we used six automated chambers with dimensions of 44.5 x 44.5 x 40.5 cm. In addition, the frame onto which the collar is placed introduces additional volume, as it is approximately 5 cm high from the peat surface. This volume is more challenging to determine accurately due to the uneven peat surface. The chambers were transparent,

made out of polymethyl methacrylate, and equipped with a lid that opened and closed automatically. Each chamber was equipped with a fan to ensure sufficient mixing of air in the chamber headspace, a soil thermometer (probe 107, Campbell Scientific, Inc., UT, USA), a PAR sensor (SQ-500, Apogee Instruments Inc., UT, USA) situated inside the chamber and a vent-tube to prevent pressure changes when opening and closing the lid. Each chamber cycle was 30 minutes and started with 5 minutes where the chamber and the tubing to and from the gas analyzer was ventilated. The chamber lid then closed for 25 minutes. The long closure time was needed to ensure a robust fit using the Keeling plot approach (Keeling, 1958). All measurements of the methane mixing ratios and $\delta^{13}C$ were performed using a Picarro G2201-i cavity ring-down spectroscopic (CRDS) analyzer (Picarro Inc., CA, USA). The chamber measurements were conducted between 07:00 – 19:00, resulting in four measurements from each chamber every day. The time between 19:00 and 07:00 was used for measurements with the NBLA approach.

The chambers were placed along a boardwalk (Figure 4). The topography of the mire is not very pronounced with the maximum difference in surface height between chamber locations being 17 cm. Furthermore, the relative elevations were not indicative for the dominant vegetation in the chambers (Table 1, Figure 5). The vegetation in the chambers falls into three categories. In chambers 1 and 2 there is a major presence of aerenchymatous sedges, typical for moist conditions in the mire. Chamber 3 is dominated by *Sphagnum* mosses, also common in moist conditions. In chambers 4 and 5 there is considerable presence of woody shrubs, typical for drier conditions. The vegetation in chamber 6 is intermediate between sedge-dominated and shrub-dominated.

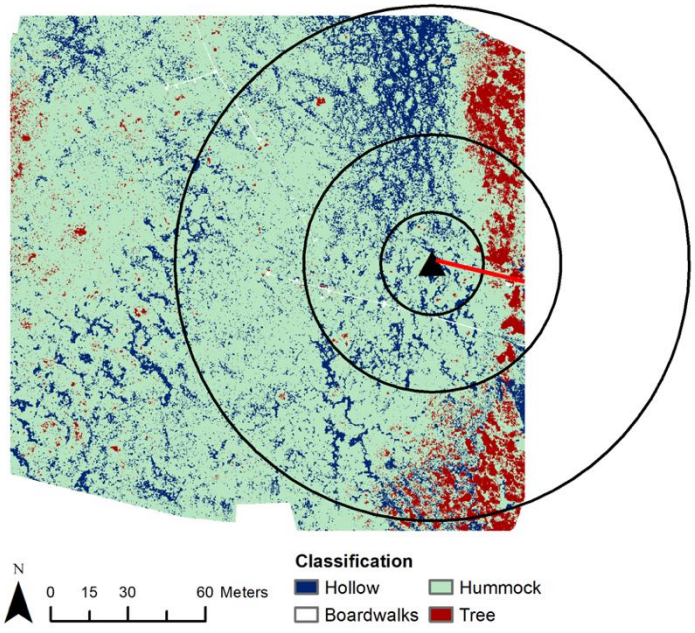

Figure 4: Distribution of dry and wet areas in Mycklemossen according to microtopography. The black triangle indicated the sampling location of measurements used for nocturnal boundary-layer accumulation (NBLA) approach. The chambers were situated along the boardwalk (red line). Black circles indicate the distances (20 m, 50 m, 100 m) from NBLA sampling point.

The emission rate of CH_4 was calculated as linear fit of CH_4 mixing ratio to time during the first 4 minutes of the closure. The first 60 seconds were discarded to avoid the disturbances at lid closure, leaving three minutes of data for the linear fitting. For data quality assurance r^2 and root-mean-square-error (RMSE) were calculated for each chamber closure. Processing and analysis of stable isotope data was conducted with MatLab (R2015b).

The $\delta^{13}C$ of the emitted CH_4 was obtained by the Keeling plot approach (Keeling, 1958). In this approach, we plotted the measured $\delta^{13}C$ against the inverse of the CH_4 mixing ratio (χ). The $\delta^{13}C$ of the emitted methane was then obtained as the intercept of the $\delta^{13}C$ value at $1/\chi = 0$, by fitting a line

$$\delta^{13}C(\chi) = a + b\chi^{-1}, \quad (1)$$

to the data. Here $\delta^{13}C(\chi)$ is the observed $\delta^{13}C$ value of CH_4 in the chamber air at the methane mixing ratio of χ, and a and b are coefficients obtained by line fitting. Coefficient a is the intercept, which will give us the isotopic signature ($\delta^{13}C$ value) of the emitted methane. The confidence interval of the $\delta^{13}C$ at intercept was obtained by the function linfitxy in MatLab (Browaeys 2021). We removed the data from closures where the uncertainty of $\delta^{13}C$ of emitted CH_4 was larger than 20 ‰.

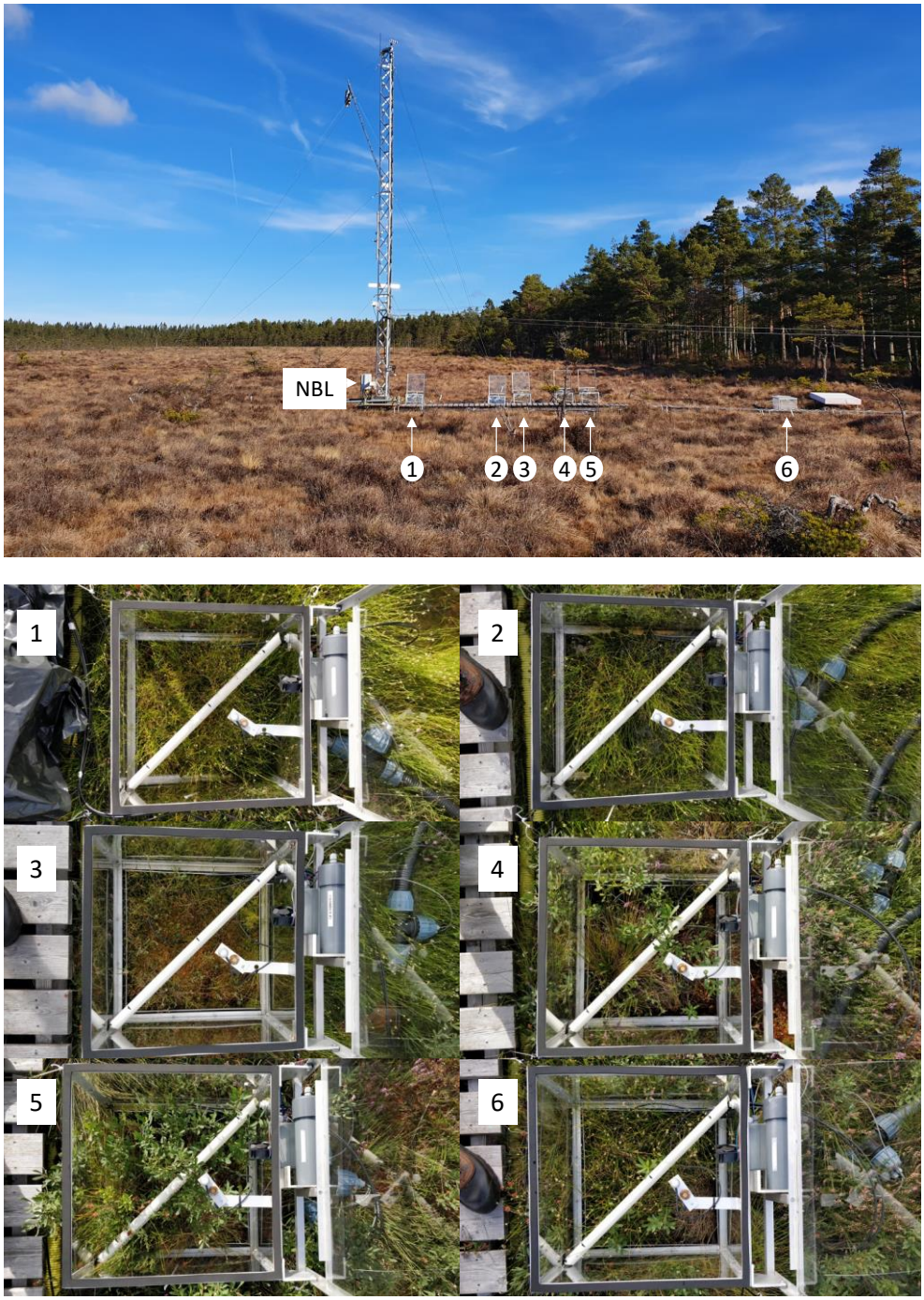

Figure 5: Top panel: Photo showing the relative location of chambers along the boardwalk. Lower panel: Photos of vegetation inside each chamber, numbered 1-6. NBL indicates the inlet for measurement of ambient air for the nocturnal boundary-layer accumulation approach.

For the NBLA approach we measured the CH_4 mixing ratio and $\delta^{13}C$ at 0.4 m above the mire surface during night-time. As the emitted CH_4 is accumulated in the shallow stable nocturnal surface layer, we can employ a similar two-end-member mixing model as for the chamber measurements (Rinne et al., 2021). Thus, we obtain the $\delta^{13}C$ of the emitted CH_4 by the Keeling plot approach (Eq. 1).

In addition to the automated measurements, we occasionally took manual air samples from chambers during closures and analyzed these with isotope ratio mass spectrometer, for comparison with the automated measurements. From each chamber closure, eight samples were taken into two liter Supel™ Inert Foil Gas Sampling bags (Sigma Aldrich, Co, LLC, USA). The eight samples from each chamber were divided into two sets, one transported to Utrecht University and the other one to Royal Holloway, University of London for analysis. The analysis methods are described by Röckmann et al. (2016) and Fisher et al. (2006). These results were compared with CRDS results and the difference in the resulting $\delta^{13}C$-CH_4 values of 3.4‰ was added to the $\delta^{13}C$-CH_4 values calculated using the CRDS data.

In order to reduce measurement noise, especially in the $\delta^{13}C$ values, we aggregated the calculated CH_4 emissions and their $\delta^{13}C$ values to ten-day averages. To analyze the spatial variability, we plotted the $\delta^{13}C$ values against CH_4 emission rates during each ten-day interval. For the analysis of temporal variation, we plotted the $\delta^{13}C$ values against the CH_4 emission rates from each chamber.

3.3 Upscaling the $\delta^{13}C$ estimates

To scale up the $\delta^{13}C$ values obtained from the different surface types by the chamber method to the isotopic signature of the whole mire, $\delta^{13}C_{mire}$, we weighted the $\delta^{13}C$ values of different surface types by the areal contribution of these surface types, and by their CH_4 emission rates,

$$\delta^{13}C_{mire} = (\sum \delta^{13}\, C_i f_i F_i)(\sum f_i F_i)^{-1}, \quad (2)$$

where $\delta^{13}C_i$ is the isotopic signature of the CH_4 emission from the surface type i, f_i is fraction of the mire covered by surface type i, and F_i is CH_4 emission rate of the surface type i. Both the $\delta^{13}C_i$ and F_i are based on the chamber measurements.

The map of mire surface types used to determine f_i in Equation 2 was based on RGB and multispectral images collected with an Unmanned Aerial Vehicle in 2017. A random forest classifier (Breiman 2001) was used to divide the mire into three vegetation classes: hummocks, hollows and trees; producing a total accuracy of 81% (see Figure 4 and Kelly et al. 2021 for more details). Table 2 shows the proportion of each surface type for different radii around the NBLA tower. In the upscaling, average $\delta^{13}C$ and CH4 emission rate from chambers 1 and 2 represented the values of wet hollows while average values

from chambers 4-6 represented those from dryer hummocks. As there were very little data from chamber 3 especially in 2020, we did not use chamber 3 for upscaling. The hollows were given areal coverage of 20% and hummocks 80%.

3.4 Genomic analysis

Peat material for genomic analysis was collected in 2018 from three different surface types specified through the wetness classification (n = 17). Using a 1.5m long box corer, peat material was cut from the oxic-anoxic interface (~5cm) and the anoxic zone (~30cm). The peat material was immediately frozen using liquid nitrogen and stored in a -80°C freezer prior to beginning gDNA extraction. The genetic DNA (gDNA) was extracted from 0.25 mg of peat following the DNeasy® PowerSoil® Kit manufacturer's protocol (Qiagen, Hilden, Germany).

The extracted gDNA was hybridized to a set of custom designed oligonucleotide probes which enrich the gene sequences related to CH_4 metabolism. This was achieved using the "captured metagenomics" method. Briefly, genes encoding enzymes related to the CH_4 production and consumption were identified in the Kyoto Encyclopedia of Genes and Genomes database (KEGG) (Kanehisa et al., 2015) and were downloaded via a custom R script (https://github.com/dagahren/metagenomic-project). The target sequences downloaded from KEGG were used to design custom hybridisation-based probes for sequence capture based on the MetCap pipeline (Kushwaha et al., 2015). For further details on probe design, library construction and sequencing refer to White et al. (2022).

Libraries were multiplexed in pools of 15 in equimolar amounts based on the concentrations and sizes of samples. 1 μg of each pool was transferred to a capture tube where target gDNA was hybridised to the custom probes according to the NimbleGen SeqCap EZ SR User's Guide (Version 4.3, October 2014). The captured libraries were sequenced on an Illumina HiSeq4000 platform using sequencing by synthesis technology to generate 2 x 150 base pair paired-end reads.

Following sequencing, raw fastq files were trimmed for the presence of Illumina adapter sequences using Cutadapt version 1.2.1 (Martin, 2011). The reads were further trimmed using Sickle version 1.200 with a minimum window quality score of 20 (Joshi, 2011). The sequence reads from each of the captured data set were submitted to MG-RAST, an online metagenomic annotation program using default parameters (Meyer et al., 2008). The taxonomic abundances were annotated using the RefSeq database (O'Leary et al., 2016) Following annotation, taxa were filtered for off-target sequences leaving only abundances of methanogenic and methanotroph microbial communities using the built in taxonomic filter within MG-RAST analysis page.

The relative abundance of methanogens and methanotrophs was calculated via the phyloseq package v1.3.0 (McMurdie and Holmes, 2013). To allow for the small samples size and uneven distribution of replicates, a PERMANOVA was used with

999 permutations (Anderson, 2001) to identify significant differences between categories. Following double root transformation, we calculated ordination using Bray-Curtis distances and finally, a Wilkson pairwise post-hoc test was used to identify significant differences between the different wetness categories via the vegan package v2.5 (Oksanen et al., 2019). All genetic analysis was completed in R statistics package v 3.6.1 (R Core Team, 2018) and visualized using the ggplot2 package v 3.3.2 (Villanueva and Chen, 2019).

4 Results

4.1 Climate

The average daily air temperatures at the mire range from slightly below zero to above 20°C (Figure 6). Water table is typically drawn down during early summer, before being replenished by late summer and autumn rains (Figure 6). In 2018, the mire was affected by a severe heatwave and drought, as shown by the long duration of the water table drawdown, as well as from the high air temperatures that summer. The years 2019 and 2020, during which the measurements reported here were conducted, we closer to average conditions.

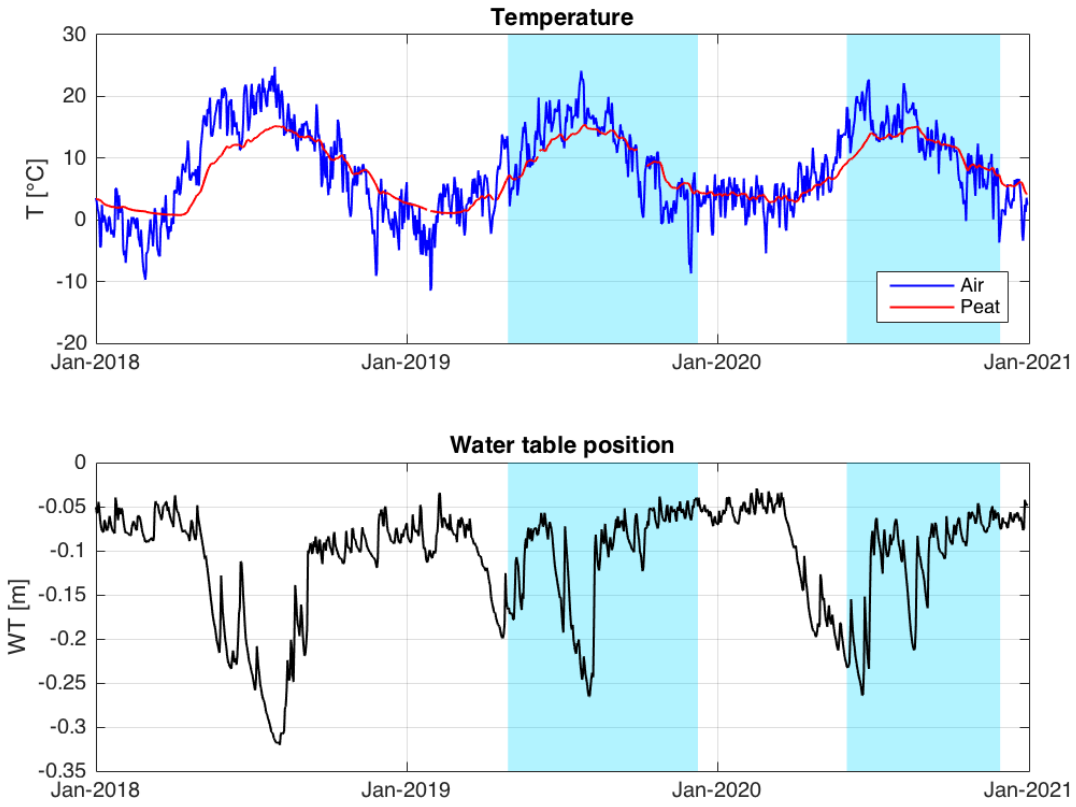

Figure 6: Meteorological conditions during 2018-2020. Periods of $\delta^{13}C\text{-}CH_4$ and F_{CH4} measurements are indicated by blue shading.

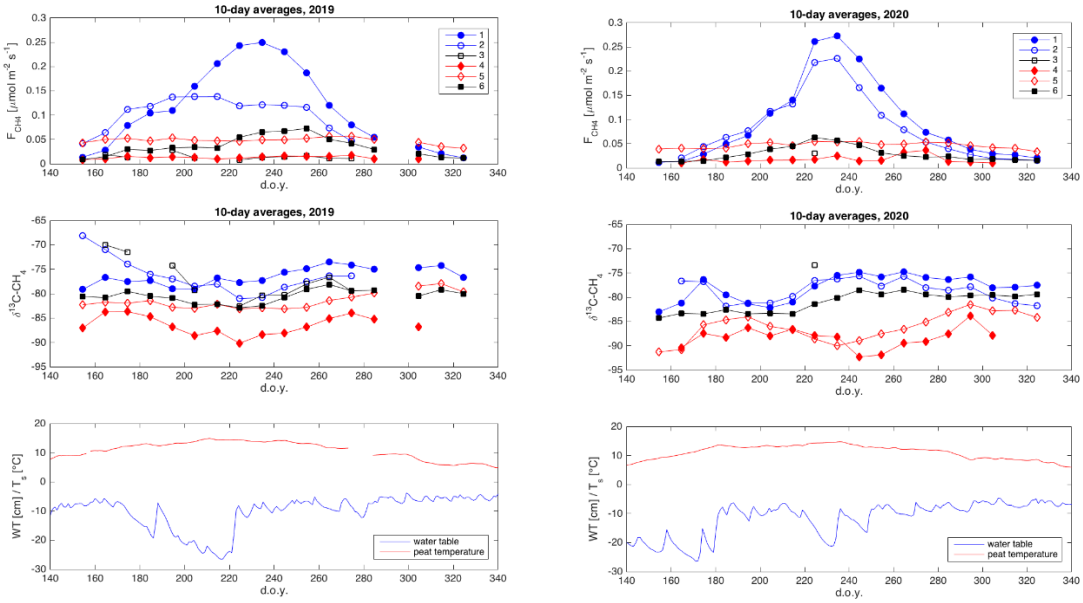

Figure 7: Time series of ten-day averages of methane emission and δ^{13}C-CH$_4$ measured from the six chambers, and peat temperature at 30 cm depth and water table position in 2019 and 2020.

4.2 CH$_4$ emission rates and δ^{13}C values

The time series of CH$_4$ emission rates from most chamber locations shows a typical seasonal cycle of CH$_4$ emission, with the highest emission rates in late summer (Figure 7; Supplementary material Figure S1). We see also distinct differences between the emission rates from different chambers indicating strong small-scale spatial variation in CH$_4$ emission rate. The highest emission rates are observed from chambers 1 and 2, with abundant aerenchymatous sedges. Chambers 3 and 4 have very low CH$_4$ emission rates, despite differences in vegetation, while 5 and 6 have intermediate emission rates. Emission rate from chamber 5 has a less pronounced annual cycle than from the other chambers.

The δ^{13}C values of emitted CH$_4$ also show relatively large differences depending on chamber location (Figure 7, Supplementary material Figure S2). In general, chamber locations with high emission rates have less depleted (less negative) δ^{13}C values of emitted CH$_4$. The seasonal cycle of the δ^{13}C values is much less obvious or systematic than that of the CH$_4$ emission rate.

The δ^{13}C values and CH$_4$ emission rates generally show a positive spatial relationship during many of the 10-day periods (Figure 8, A1 and A2). The positive relationship was more pronounced during the period of high emission rates (doy 200-

260), and more evident in 2019 than in 2020. However, chamber 3 deviated consistently during 2019 from the general behavior of the other chambers. Unfortunately, there were hardly any data that passed the quality assurance and control criteria from that chamber during 2020 due to low CH_4 emission rates. Omitting the data from chamber 3 led to statistically significant correlations between CH_4 emission rate and its $\delta^{13}C$ value during many of the 10-day periods (Fig. 8).

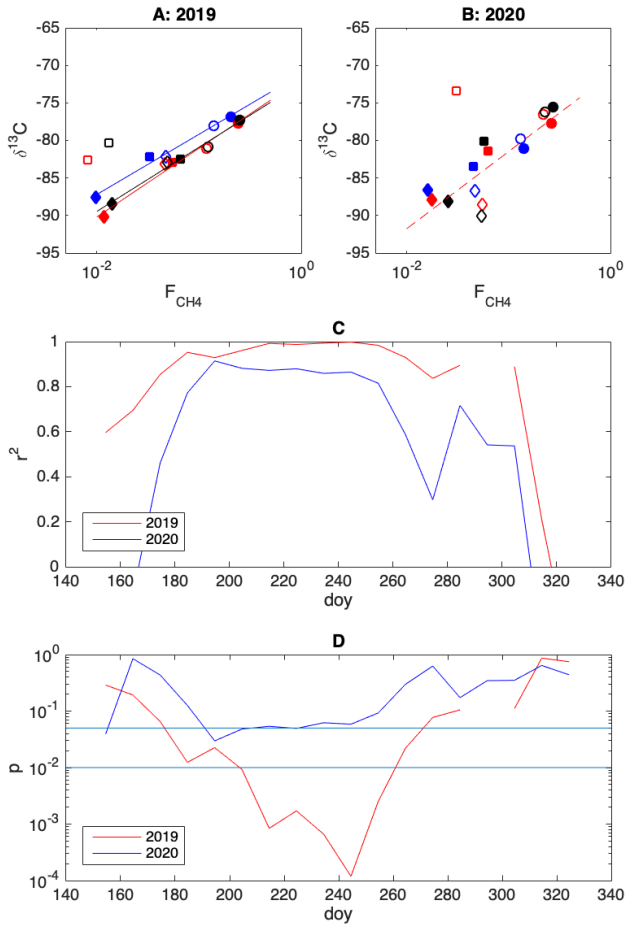

Figure 8: Panels A and B: Examples of spatial variation of ten-day averages of $\delta^{13}C$-CH_4 against F_{CH4}, during three ten-day time periods in 2019 and 2020. Chambers: 1, solid circles; 2, open circles; 3: open squares; 4: solid diamonds; 5: open diamonds; 6: solid squares. Colors of markers and lines indicate period: day of year (doy) 210-219, red; doy 220-229, blue; doy 230-239, black. Solid line indicates correlation with $p<0.01$, dashed line with $p<0.05$. Panel C: r^2 between ten-day averages of $\delta^{13}C$ and F_{CH4}, without chamber 3. Panel D: p-value of correlation, without chamber 3.

The temporal relation of $\delta^{13}C$ values and CH_4 emission rates showed a hysteresis-like behavior at three of the measurement locations (chambers 1, 2 and 6) during 2020 and at two locations (chambers 1 and 6) in 2019 (Figure 9). These locations are either wet or intermediate sites with relatively high emission rates. In these locations, the $\delta^{13}C$ values of emitted CH_4 were lower in the early part of the growing season than during a period with similar emission rates later in the season. The dry sites with lower CH_4 emission did not show observable systematic behavior in their $\delta^{13}C$ - CH_4 emission rate relation.

The $\delta^{13}C$ values of emitted CH_4 derived by the nocturnal boundary layer method are in the same range as the $\delta^{13}C$ values observed at the wet and intermediate chambers, with some similarities in their seasonal cycle (Figure 10, S3). The upscaling of the chamber data using the microtopographic map resulted in an average $\delta^{13}C$ value of emitted CH_4 of -81.3 ‰. The average $\delta^{13}C$ value of emitted CH_4 according to NBLA measurements was -79.3 ‰.

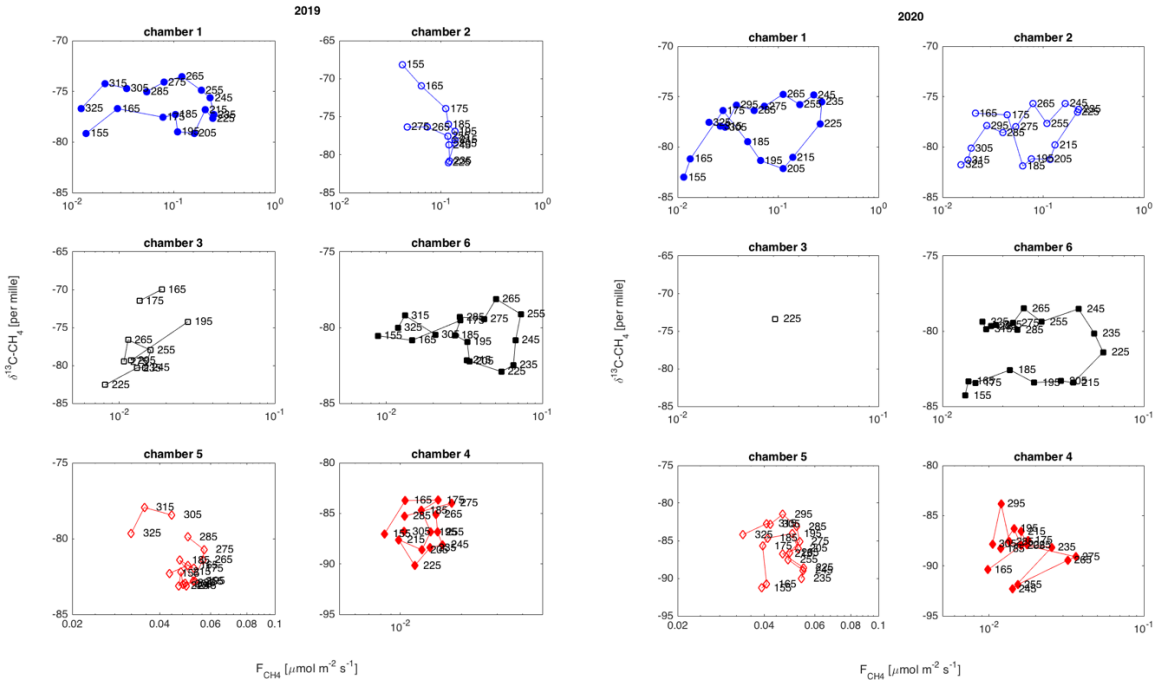

Figure 9: Temporal variation of $\delta^{13}C$-CH_4 against F_{CH4}, in each chamber location in 2019 and 2020. The marker labels indicate the day of year. Only very few data points in from chamber 3 passed the quality criteria in 2020, resulting in only one ten-day average.

4.3 Genomic analysis

In total, 20 methanogens and five methanotrophs were identified at *genus* level. *Genera* were spread across four classes of methanogens including Methanobacteria, Methanococci, Methanomicrobia and Methanopyri. In addition, three classes of methanotrophs including type I Gammaproteobacteria, type II Alphaproteobacteria and Verrucomicrobia were also detected. These *genera* included methanogens with the ability to perform methanogenesis via all metabolic pathways including hydrogenotrophic, acetoclastic, methylotrophic and the specialist methanogen, *Methanosarcina* (Hydr/Methyl/Aceto methanogen), which holds the ability to metabolize via multiple alternative pathways.

The proportion of methanogens to methanotrophs is a 58% to 42% split when combining all the samples. The dominant methanogens were hydrogenotrophic methanogens (46%), followed by the multiple metabolic pathway genus *Methanosarcina* (10%), with the methylotrophic and acetoclastic methanogens contributing 2% and ≤ 1% respectively. The dominant methanotrophs were the type II Alphaproteobacteria (30%), followed by type I Gammaproteobacteria (8%) and Verrucomicrobia (4%).

Significant variation in the relative abundance of taxa was observed between the wet, intermediate and dry categories ($p \leq 0.02$) (figure 11). The PERMANOVA indicated that 37% of the variation in taxa was explained by the wetness category (R^2 0.37, $p \leq 0.02$). When testing pairwise between categories, significant differences occurred between wet - dry ($p \leq 0.04$) and wet - intermediate categories ($p \leq 0.04$), but not between the dry - intermediate categories ($p \geq 0.05$).

The functional group contributing the most to dissimilarity in all comparisons was the hydrogenotrophic methanogens, with an average dissimilarity of 0.29 ± 0.19 SD between intermediate - wet, 0.20 ± 0.16 SD between intermediate - dry and finally, 0.30 ± 0.17 SD between wet - dry categories (Tables 3, 4, 5). Although contributing the highest to dissimilarity the difference was identified as non-significant when comparing between categories. Type II methanotrophs, multiple metabolic pathway Methanosarcina, Type I methanotrophs and hydrogenotrophic methanogens contributed second, third, fourth and fifth to dissimilarity, respectively. Interestingly, methylotrophic methanogens contributed little to dissimilarity but were the only methanogenic functional group to be significantly higher in abundance in wet locations when compared to intermediate ($p \leq 0.027$) and dry plots ($p \leq 0.046$). Type I methanotrophs and Verrucomicrobia methanotrophs had significantly higher average abundance in wet locations when compared to intermediate ($p \leq 0.01$) and dry plots ($p \leq 0.004$). However, type II methanotrophs were only significantly higher in abundance in wet plots when compared to dry ($p \leq 0.036$).

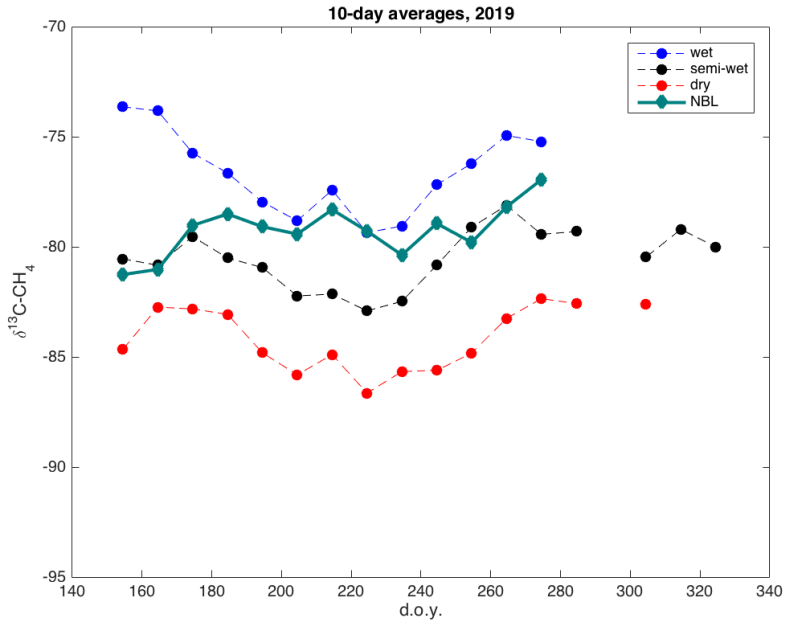

375

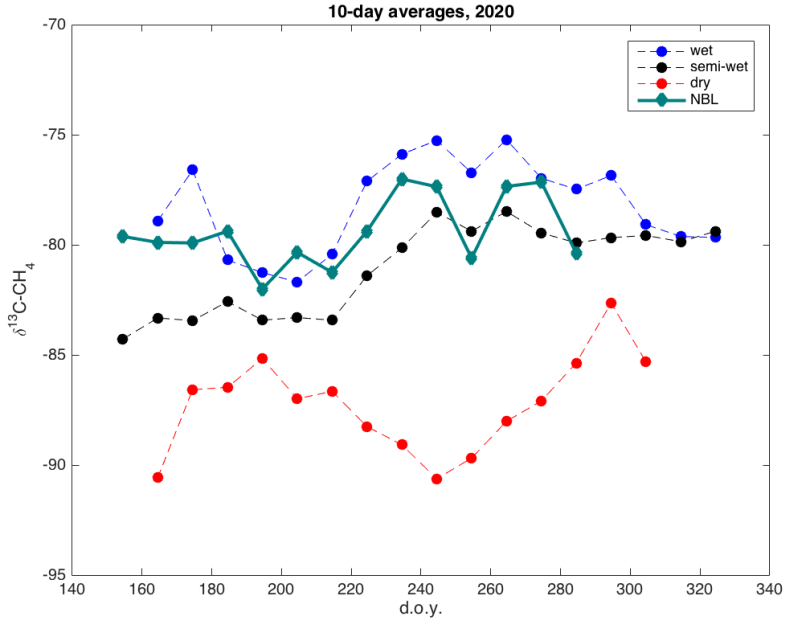

Figure 10: Time series of ten-day average $\delta^{13}C\text{-}CH_4$ derived by nocturnal boundary-layer Keeling plot approach (green), and averages of wet (blue), intermediate (black) and dry (red) locations, for 2019 and 2020.

380

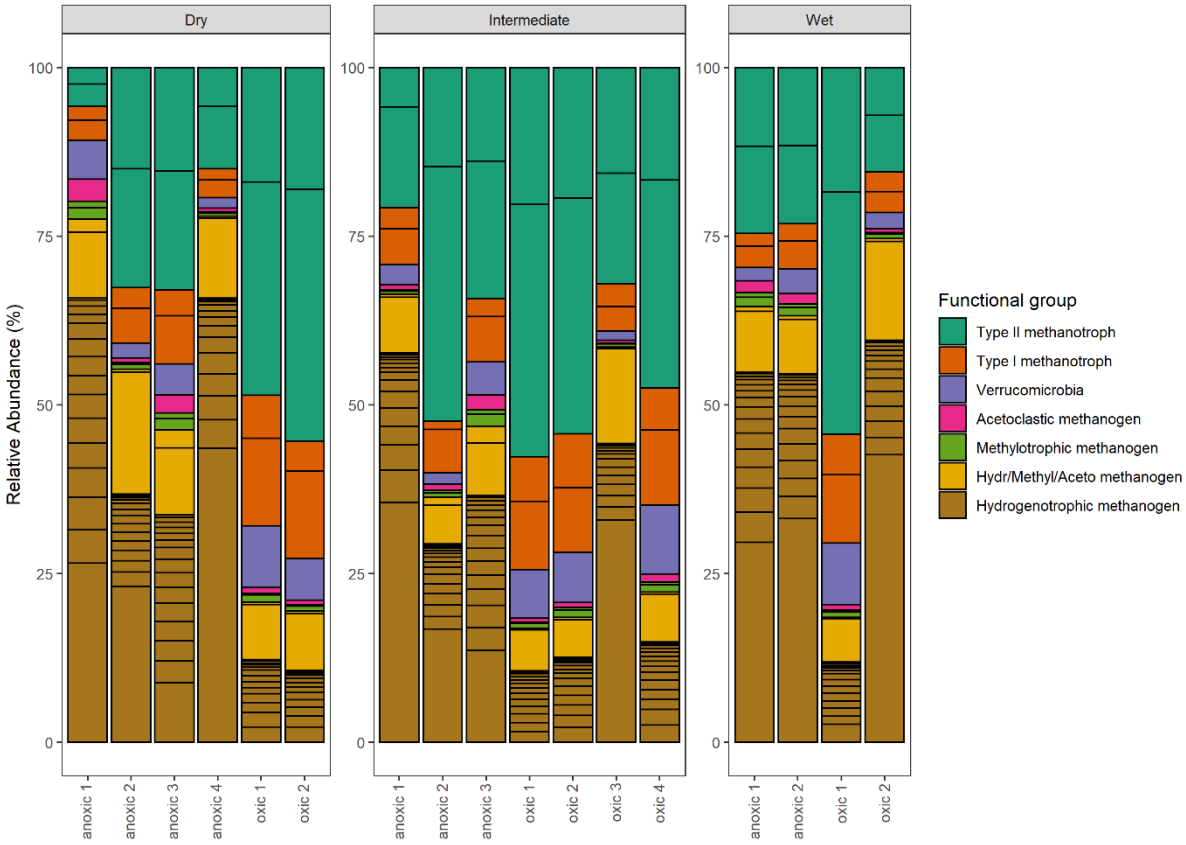

Figure 11: Taxonomic composition: The relative abundance (%) of methanogenic and methanotrophic microbes at genus level. Color indicates functional group and which metabolic pathway is utilized during metabolism.

5 Discussion

385 The CH_4 emitted from surfaces covered by different vegetation types show large differences in its $\delta^{13}C$ values. In the late summer of 2020, the differences between the 10-day average $\delta^{13}C$ values from different chambers were up to 10-15 ‰. Considering the modest microtopography of Mycklemossen mire, and the closeness of the measurement locations (Table 1, Figure 10), this indicates a considerable small-scale spatial variation in the processes leading to CH_4 emission. Our findings are in line with the large observed differences in CH_4 emission rates due to small-scale spatial variability from other mire
390 ecosystems (e.g. Riutta et al., 2007; Keane et al., 2021). The spatial variation of $\delta^{13}C$ values observed at Mycklemossen are in the same range with that observed at Abisko-Stordalen mire (68°20'N, 19°30'E) in Northern Sweden by McCalley et al.

(2014). Furthermore, McCalley et al. (2014) and Mondav et al. (2017) identified the same genera of hydrogenotrophic methanogens in Abisko-Stordalen mire which we found at Mycklemossen, with the same genus (*Methanoregula*) being dominant. The similar range of the $\delta^{13}C$ values and similar methanogens at Mycklemossen and Abisko-Stordalen mires is interesting as these mires are located over 1100 km apart and differ considerably in their microtopography and climate. The microtopographic height differences at Abisko-Stordalen are about a meter, as compared to about 20 cm at Mycklemossen. Furthermore, due to the cold climate and thin wintertime snow cover Abisko-Stordalen features discontinuous permafrost in the form of palsas, whereas Mycklemossen is a temperate non-permafrost mire.

The spatial variation in the $\delta^{13}C$ values of emitted CH_4 is systematic over the growing season and two years of measurements. Generally, the wet sedge-dominated plots with higher emission rates are associated with higher $\delta^{13}C$ values, and the dry shrub-dominated plots with lower emission rates with lower $\delta^{13}C$ values, indicating the likely importance of substrate availability and methanogenesis in determining the spatial variation in the CH_4 emission rate. Similar spatial relations between $\delta^{13}C$ and CH_4 emission rate have been observed by e.g. Hornibrook and Bowes (2007) in Welsh mires, and by McCalley et al. (2014) in a Swedish subarctic Abisko-Stordalen mire. However, the position of the chamber 3 in the $\delta^{13}C$ - CH_4 emission rate diagram (Fig 8, A1, A2), suggests an effect of methanotrophy on CH_4 emission and its $\delta^{13}C$ value from this location. This may be due to the dominance of Spaghnum mosses in this chamber, which have been shown to support considerable methanotrophy (Larmola et al., 2010). The significantly higher abundance of type II methanotrophs in wetter locations as compared to dry and intermediate supports this suggestion.

Of our two hypotheses on the origins of the spatial variation of CH_4 emission rates, one (HS1) assumes methanotrophy to be the key explanatory process while the other (HS2) assumes substrate availability to drive the spatial variation. The relation between the CH_4 emission rate and $\delta^{13}C$ values of emitted CH_4 we observed, especially at locations with vascular vegetation cover, mostly corroborates the latter hypothesis (HS2). Corroboration of the HS1 hypothesis would have required a negative correlation between the $\delta^{13}C$ and CH_4 emission rate. Furthermore, the presence of hydrogenotrophic, acetoclastic and methylotrophic methanogens enables the community to utilize all substrates available. Thus, it is unlikely that methanotrophy plays a major role in explaining the spatial variation of CH_4 emission from this mire system, especially as the moss dominated areas seem to cover a minor area of the mire.

As it is possible that there are seasonal differences in the factors affecting the spatial variability of the methane emission (temperature, substrate availability, methanotrophy), we analyzed the spatial variation throughout the growing seasons as ten-day averages. According to the observed spatial relations between $\delta^{13}C$ and CH_4 emission rates during these two growing seasons there were no major temporal shifts in the behavior of the $\delta^{13}C$ - CH_4 emission rate relationship (Figures A1 and A2). The $\delta^{13}C$ values and CH_4 emission rate, omitting chamber 3, showed tendency for positive correlation for most of the

growing seasons. Thus, it seems that the processes leading to the spatial variations in CH_4 emission are similar throughout the growing season.

The temporal variation in $\delta^{13}C$ was smaller and less systematic than its spatial variation. Interestingly, this temporal relation does not show similar systematic behavior than the spatial variation, indicating that the space-for-time analogy may not be valid in these seasonal time scales. The temporal behavior of $\delta^{13}C$ in relation to CH_4 emission rate shows a hysteresis-like behavior at some of the chamber plots. The hysteresis-like behavior is clear in wet or intermediate plots with high emission rates. The lack of observable hysteresis-like behavior in the other plots could be due to the small range of emission rates leading to random variation in the data to mask the any systematic behavior. The hysteresis-like behavior indicates that the temporal variation of CH_4 emission rates from this mire could be a result of two time-lagged compounding effects, following the HT3 hypothesis, especially as the variation of $\delta^{13}C$ value and CH_4 emission rate in mire-scale are mostly affected by the high-emitting surfaces. The increasing CH_4 emissions during the first half of the growing season could be caused by increasing peat temperature enhancing the activity of methanogenic Archaea (Juottonen et al., 2008). Later in the growing season, the increased input of root exudates from vascular plants would increase the substrate availability, resulting in higher $\delta^{13}C$ values than in the early season, yet similar CH_4 emission rates. However, we cannot assign the whole seasonal cycle of CH_4 emission rates to changes in substrate availability, as this would result in a pronounced positive relationship between $\delta^{13}C$ and CH_4 emission rates, which we did not observe. According to the genetic analysis, the microbial community holds the functional potential to produce CH_4 via the hydrogenotrophic and acetoclastic pathways, thus enabling shifts in $\delta^{13}C$ following the seasonal changes in availability of substrate. However, the highly depleted $\delta^{13}C$ does indicate dominance of hydrogenotrophic methane production at this mire, with changes in $\delta^{13}C$ of emitted CH_4 due to energetics of this process (Penning et al., 2005; Hornibrook 2009). Thus, the hysteresis between temperature and CH_4 emission, similar to that observed by Chang et al., (2020; 2021) and Łakomiec et al. (2021), could be partly due to the seasonal development of peat temperature and partly due to the changes in substrate availability for methane production.

The $\delta^{13}C$ values of emitted CH_4 derived by the nocturnal boundary-layer approach (NBLA) corresponded in magnitude to the values of the wet and intermediate surfaces. As these surfaces dominate the emission, it is natural that the NBLA approach will correspond to these more closely than to the dry surfaces with low CH_4 emission. The up-scaled $\delta^{13}C$ from the chamber measurements was in a similar range to the mire-scale $\delta^{13}C$ measured by the NBLA method, indicating the dominance of hydrogenotrophic methanogenetic pathways. Obtaining reliable mire scale isotopic signatures is crucial, for example for the use of isotopic data for source apportioning of CH_4 by atmospheric inversions. Here we show that the chamber $\delta^{13}C$ measurements can be successfully upscaled using a mire surface characterization based on UAV data. Such an approach enables the calculation of mire-scale $\delta^{13}C$ estimates at sites where NBLA measurements are not available. In combination

with UAV-upscaled CO_2 fluxes (e.g. Kelly et al 2021), there are further opportunities to examine the impacts of spatial variations in vegetation productivity and respiration on CH_4 emission rates and $\delta^{13}C$ values.

The mire scale $\delta^{13}C$ value of emitted CH_4 observed at Mycklemossen (-81‰ to -79‰) is somewhat lower than observations in northern Scandinavia by Fischer et al., (2017) and in the lower end of the wetland $\delta^{13}C$-CH_4 distribution as presented by Menoud et al., (2022). All these show considerably lower $\delta^{13}C$ values of CH_4 emitted from northern mire ecosystems than the average $\delta^{13}C$ values for wetland CH_4 emissions used in many atmospheric inversion studies (-60‰ to -58‰; Mikaloff-Fletcher et al., 2004a,b; Bousquet et al., 2006; Monteil et al., 2011). Together with the wider data sets of Fisher et al., (2017) and Menoud et al. (2022), the observations presented here would support using a lower $\delta^{13}C$ value for CH_4 emitted from northern mire ecosystems in atmospheric inversion studies.

6 Conclusions

We conducted automatic chamber and nocturnal boundary layer (NBLA) measurements of $\delta^{13}C$ values of emitted CH_4, as well as genomic analyses of the CH_4-relevant microbial communities, to investigate the drivers of the spatial and temporal variability of CH_4 emission rate and $\delta^{13}C$ value in a temperate Swedish mire. Despite the small elevation differences (<20 cm) between the microtopographic zones in the mire, we observed stark contrasts in the CH_4 emission rates and $\delta^{13}C$ values between the zones, similar in magnitude to mires which have much more pronounced microtopography. According to the relationships between $\delta^{13}C$ values and CH_4 emission rates we observed, the spatial variability of CH_4 emission from Mycklemossen mire is unlikely to be controlled mostly by methanotrophy. Instead, variations in methanogenesis due to the differences in substrate availability, following our hypothesis 2 on spatial variability (HS2), seem to be a more likely source of most of the variation in CH_4 emission rates. The seasonal variation of CH_4 emission is likely controlled by both temperature and substrate availability, leading to hysteresis-like behavior in the $\delta^{13}C$ - CH_4 emission rate relationship, following our hypothesis 3 on temporal variability (HT3). The taxonomic data shows the functional potential to produce CH_4 via multiple metabolic pathways, enabling shifts following changes the substrate availability. However, the highly depleted $\delta^{13}C$ values observed indicate the dominance of hydrogenotrophic methanogenesis, and thus the variation in $\delta^{13}C$ may be due to the energetics of this process. Interestingly, the measurement plot with Sphagnum-dominated vegetation diverged from the general spatial $\delta^{13}C$-F_{CH4} relation, warranting future studies on this vegetation type. In addition, we confirmed that drone-based upscaling of $\delta^{13}C$ chamber measurements provides reliable mire-scale estimates when compared to NBLA $\delta^{13}C$ estimates. The observed mire scale $\delta^{13}C$ values were in the lower end of reported $\delta^{13}C$ values from northern mires and together with these, support the need for revising the $\delta^{13}C$ value for northern wetland systems used in atmospheric inversion studies. The results obtained can help to constrain our theories on the causes of the variability of methane emission from

mire ecosystems and can thus be useful in development of numerical models of mire biogeochemistry, needed to predict the fate of northern mire ecosystems in the changing climate.

Appendix A: Spatial δ^{13}C-CH$_4$ - F$_{CH4}$ relations as ten-day averages

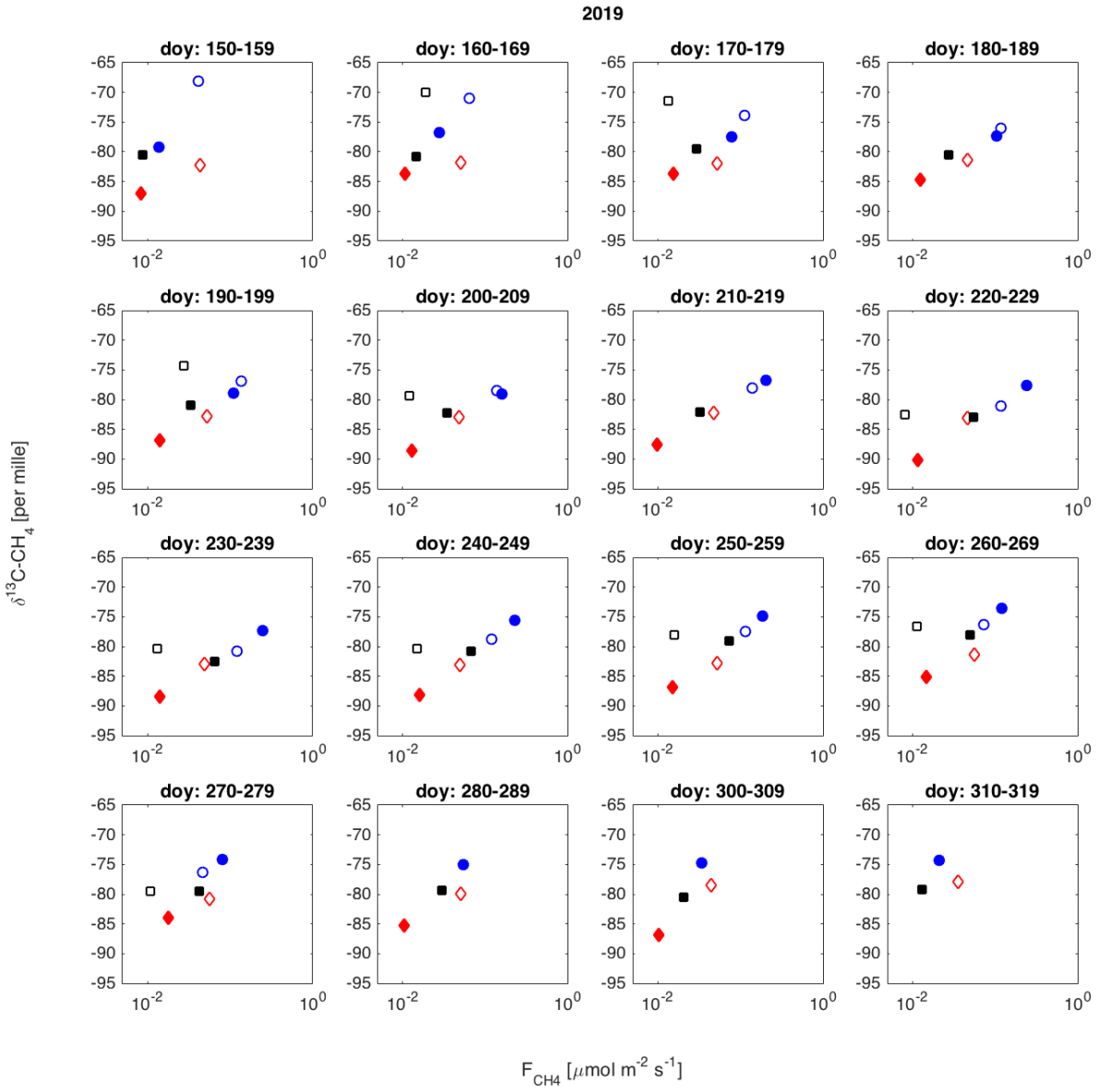

Figure A1: Spatial variation of δ^{13}C-CH$_4$ against F$_{CH4}$, as ten-day averages during 2019. Chamber 1: blue solid circle; 2: blue open circle; 3: black open square; 4: red solid diamond; 5: red open square; 6: black solid square.

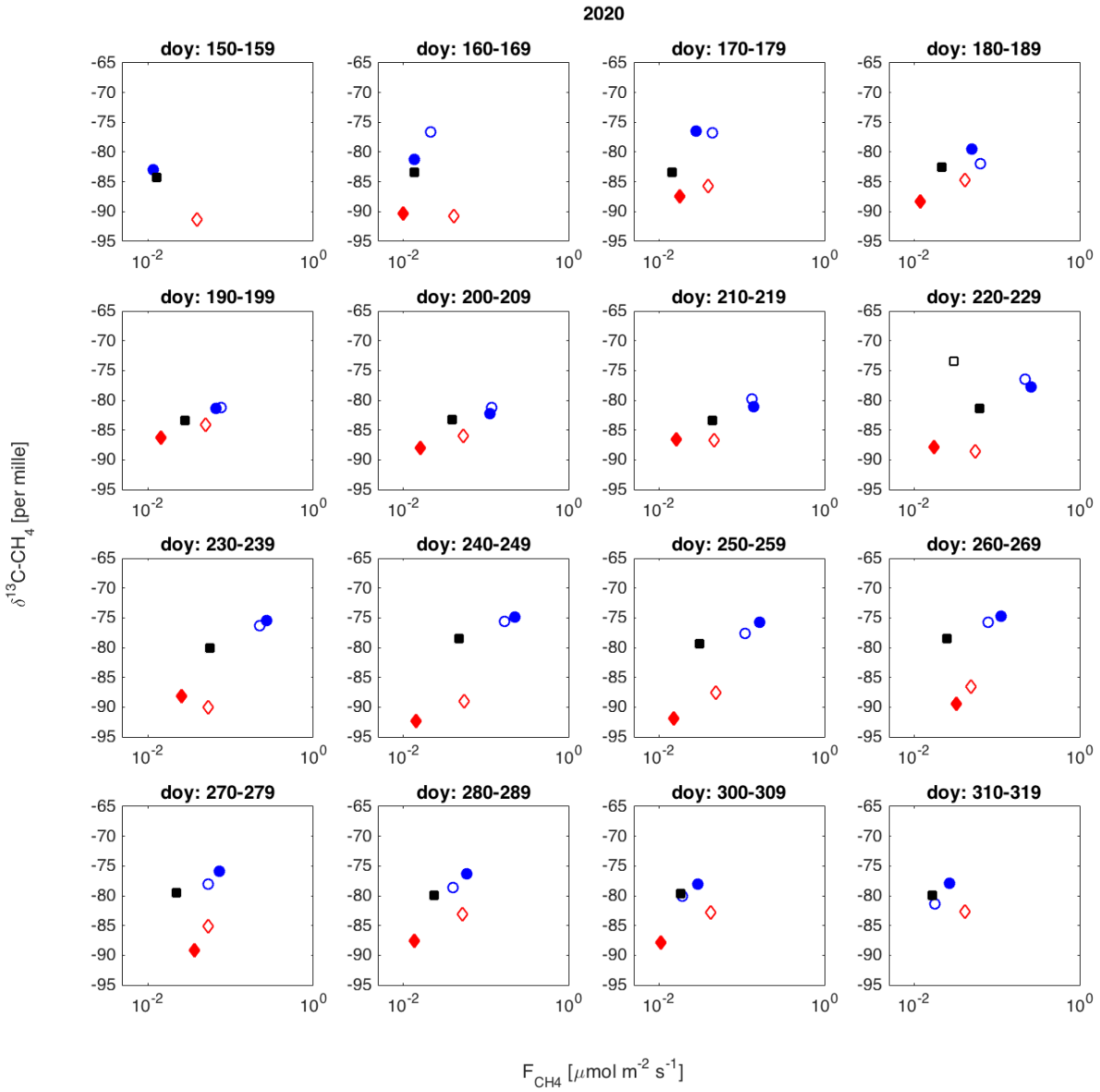

495

Figure A2: Spatial variation of δ^{13}C-CH_4 against F_{CH4}, as ten-day averages during 2020. Chamber 1: blue solid circle; 2: blue open circle; 3: black open square; 4: red solid diamond; 5: red open square; 6: black solid square.

Acknowledgements

We thank Malika Menoud and Prof. Thomas Röckmann at IMAU, and Dr. David Lowry at RHUL for help in isotopic analysis of bag samples. The access to the Mycklemossen site was made possible by Swedish Infrastructure for Ecosystem Sciences (SITES, co-financed by the Swedish Research Council) and ICOS Sweden network (co-financed by the Swedish Research Council (grant no. 2015-06020, 2019-00205). Probe hybridization and sequencing was performed at the Center for Genomic Research, University of Liverpool. Data handling was enabled by resources in project (SNIC 2019/8-365) provided by the Swedish National Infrastructure for Computing (SNIC) at UPPMAX, partially funded by the Swedish Research Council through grant agreement no. 2018-05973.

Financial Support

This research has been supported by the MEthane goes Mobile: MEasurement and MOdeling (MEMO2) project from the European Union's Horizon 2020 research and innovation program under the Marie Skłodowska-Curie grant no. 722479. We acknowledge Crafoord foundation for financial support for financing the Picarro isotope analyzer. We acknowledge funding from Strategic Research Area BECC (2018).

Data availability

The annotated metagenomes are available at the MG-RAST server under the project ID: 91145. The isotopic and methane emission data is available at zenodo: 10.5281/zenodo.6385096

Code availability

Code used in the taxonomic analysis can be found at https://github.com/joel332/Analysis-of-captured-metagenomic-data/blob/main/Mycklemossen_isotopes_taxanomic_analysis. The code for methane flux and isotopic analysis is available at zenodo: 10.5281/zenodo.6670314.

References

Anderson, M. J.: A new method for non-parametric multivariate analysis of variance. Austral Ecology, 26, 32-46, 2001.

Bousquet, P., Ciais, P., Miller, J.B., Dlugokencky, E.J., Hauglustaine, D.A., Prigent, C., Van der Werf, G.R., Peylin, P., Brunke, E.G., Carouge, C., Langenfelds, R.L., Lathiere, J., Papa, F., Ramonet, M., Schmidt, M., Steele, L.P., Tyler, S.C.,

and White, J.: Contribution of anthropogenic and natural sources to atmospheric methane variability. Nature 443, 439-443, 2006.

Breiman, L.: Random Forests. Machine Learning, 45, 5–32, 2001.

Brix, H., Sorrell, B.K., and Orr, B.T.: Internal pressurization and convective gas-flow in some emergent fresh-water macrophytes. Limnology and Oceanography, 37, 1420–1433. https://doi.org/10.4319/lo.1992.37.7.1420, 1992.

Chang, K.-Y., Riley, W.J., Crill, P.M., Grant, R.F., and Saleska, S.R.: Hysteretic temperature sensitivity of wetland CH4 fluxes explained by substrate availability and microbial activity. Biogeosciences, 17, 5849–5860, 2020.

Chang, K.-Y., Riley, W.J., Knox, S.H., Jackson, R.B., McNicol, G., Poulter, B., Aurela, M., Baldocchi, D., Bansal, S., Bohrer, G., Campbell, D.I., Cescatti, A., Chu, H., Delwiche, K.B., Desai, A., Euskirchen, E., Friborg, T., Goeckede, M., Helbig, M., Hemes, K.S., Hirano, T., Iwata, H., Kang, M., Keenan, T., Krauss, K.W., Lohila, A., Mammarella, I., Mitra, B., Miyata, A., Nilsson, M.B., Noormets, A., Oechel, W.C., Papale, D., Peichl, M., Reba, M.L., Rinne, J., Runkle, B.R.K., Ryu, Y., Sachs, T., Schäfer, K.V.R., Schmid, H.P., Shurpali, N., Sonnentag, O., Tang, A.C.I., Torn, M.S., Trotta, C., Tuittila, E.-S., Ueyama, M., Vargas, R., Vesala, T., Windham-Myers, L., Zhang, Z., and Zona, D.: Substantial hysteresis in emergent temperature sensitivity of global wetland CH4 emissions. Nature Communications, 12, 2266, 2021.

Chanton, J. P., Chaser, L. C., Glaser, P., and Siegel, D.: Isotopic Effects Associated with Methane Production Mechanisms. (In: Flanagan, et al. Eds Stable Isotopes and Biosphere-Atmosphere Interactions), Elsevier, pp. 85–105, 2005.

Ciais, P., Sabine, C., Bala, G., Bopp, L., Brovkin, V., Canadell, J., Chhabra, A., DeFries, R., Galloway, J., Heimann, M., Jones, C., Le Quéré, C., Myneni, R.B., Piao S., and Thornton, P.: Carbon and Other Biogeochemical Cycles. In: Climate Change 2013: The Physical Science Basis. Contribution of Working Group I to the Fifth Assessment Report of the Intergovernmental Panel on Climate Change [Stocker, T.F., D. Qin, G.-K. Plattner, M. Tignor, S.K. Allen, J. Boschung, A. Nauels, Y. Xia, V. Bex and P.M. Midgley (eds.)]. Cambridge University Press, Cambridge, United Kingdom and New York, NY, USA, 2013.

Fisher, R., Lowry, D., Wilkin, O., Sriskantharajah, S., and Nisbet, E.G.: High-Precision, Automated Stable Isotope Analysis of Atmospheric Methane and Carbon Dioxide Using Continuous-Flow Isotope-Ratio Mass Spectrometry, Rapid Communications in Mass Spectrometry, 20, 200–208, https://doi.org/10.1002/rcm.2300, 2006.

Fisher, R.E., France, J.L., Lowry, D., Lanoisellé, M., Brownlow, R., Pyle, J.A., Cain, M., Warwick, N., Skiba, U.M., Drewer, J., Dinsmore, K.J., Leeson, S.R., Bauguitte, S.J.-B., Wellpott, A., O'Shea, S.J., Allen, G., Gallagher, M.W., Pitt, J., Percival, C.J., Bower, K., George, C., Hayman, G.D., Aalto, T., Lohila, A., Aurela, M., Laurila, T., Crill, P.M., McCalley, C.K., and Nisbet, E.G.: Measurement of the 13C isotopic signature of methane emissions from northern European wetlands, Global Biogeochem. Cycles, 31, 605–623, doi:10.1002/2016GB005504, 2017.

Heiskanen, J., Brümmer, C., Buchmann, N., Calfapietra, C., Chen, H., Gielen, B., Gkritzalis, T., Hammer, S., Hartman, S., Herbst, M., Janssens, I.A., Jordan, A., Juurola, E., Karstens, U., Kasurinen, V., Kruijt, B., Lankreijer, H., Levin, I., Linderson, M.-L., Loustau, D., Merbold, L., Lund Myhre, C., Papale, D., Pavelka, M., Pilegaard, K., Ramonet, M., Rebmann, C., Rinne, J., Rivier, L., Saltikoff, E., Sanders, R., Steinbacher, M., Steinhoff, T., Watson, A., Vermeulen, A.T., Vesala, T., Vítková, G., and Kutsch, W.: Integrated Carbon Observation System in Europe. Accepted for publication in Bulletin of the American Meteorological Society, 2021a.

Heiskanen, L., Tuovinen, J.-P., Räsänen, A., Virtanen, T., Juutinen, S., Lohila, A., Penttilä, T., Linkosalmi, M., Mikola, J., Laurila, T., and Aurela, M.: Carbon dioxide and methane exchange of a patterned subarctic fen during two contrasting growing seasons. Biogeosciences, 18, 873–896, 2021b.

Hornibrook, E.R.C., The stable carbon isotope composition of methane produced and emitted from northern peatlands. In: Baird et al., (Eds.): Carbon cycling in Northern Peatlands. Geophysical Monograph, 184, 187-203, 2009

Hornibrook, E.R.C., and Bowes, H.L., Trophic status impacts both the magnitude and stable carbon isotope composition of methane flux from peatlands. Geophys. Res. Lett., 34, L21401, doi:10.1029/2007GL031231, 2007.

Jackowicz-Korczyński, M., Christensen, T.R., Bäckstrand, K., Crill, P., Friborg, T., Mastepanov, M., and Ström, L.: Annual cycle of methane emission from a subarctic peatland. Journal of Geophysical Research, 115, G02009. https://doi.org/10.1029/2008JG000913, 2010.

Joabsson, A., and Christensen, T.R.: Methane emissions from wetlands and their relationship with vascular plants. Global Change Biology, 7(8), 919–932. https://doi.org/10.1046/j.1354-1013.2001.00044.x, 2001.

Joabsson, A., Christensen, T.R., and Wallén, B.: Vascular plant controls on methane emissions from northern peatforming wetlands. TREE, 14(10), 385–388, 1999.

Joshi, N.: Sickle: A sliding-window, adaptive, quality-based trimming tool for FastQ files (Version 1.33) [Online]. Available: https://github.com/najoshi/sickle [Accessed 19-2-2020], 2011.

Juottonen, H., Tuittila, E.-S., Juutinen, S., Fritze, H., and Yrjälä, K.: Seasonality of rDNA- and rRNA-derived archaeal communities and methanogenic potential in a boreal mire. The ISME Journal, 2, 1157–1168, https://doi.org/10.1038/ismej.2008.66, 2008.

Kanehisa, M., Sato, Y., Kawashima, M., Furumichi, M., and Tanabe, M.: KEGG as a reference resource for gene and protein annotation. Nucleic Acids Research, 44, D457-D462, 2015.

Keane, B., Toet, S., Ineson, P., Weslien, P., Stockdale, J. E., and Klemedtsson, L.: Carbon dioxide and methane flux response and recovery from drought in a hemiboreal ombrotrophic bog. Frontiers in Earth Science, section Biogeoscience, 8, 562401, DOI: 10.3389/feart.2020.562401, 2021.

Keeling, C.D.: The concentration and isotopic abundances of atmospheric carbon dioxide in rural areas, Geochim. Cosmochim. Acta, 13, 322–334, 1958.

Kelly, J., Kljun, N., Eklundh, L., Klemedtsson, L., Liljebladh, B., Olsson, P.-O., Weslien, P., and Xie X.: Modelling and upscaling ecosystem respiration using thermal cameras and UAVs: Application to a peatland during and after a hot drought. Agricultural and Forest Meteorology, 300, 108330, 2021.

Kim, J., Verma, S.B., Billesbach, D.P., and Clement, R.J.: Diel variation in methane emission from a midlatitude prairie wetland: Significance of convective throughflow in Phragmites australis. Journal of Geophysical Research, 103(D21), 28,029–28,039. https://doi.org/10.1029/98JD02441, 1998.

Kowalska, N., Chojnicki, B.H., Rinne, J., Haapanala, S., Siedlecki, P., Urbaniak, M., Juszczak R., and Olejnik, J.: Measurements of methane emission from a temperate wetland by the eddy covariance method. International Agrophysics, 27, 283–290, 2013.

Kushwaha, S.K., Manoharan, L., Meerupati, T., Hedlund, K., and Ahren, D.: MetCap: a bioinformatics probe design pipeline for large-scale targeted metagenomics. BMC Bioinformatics, 16, 65, 2015.

Lai, D.Y.F.: Methane Dynamics in Northern Peatlands: A Review. Pedosphere, 19, 409-421, 2009.

Łakomiec, P., Holst, J., Friborg, T., Crill, P., Rakos, N., Kljun, N., Olsson, P.-O., Eklundh, L., Persson A., and Rinne, J.: Field-scale CH4 emission at a sub-arctic mire with heterogeneous permafrost thaw status. Biogeosciences. 18, 5811–5830, 2021.

Larmola, T., Tuittila, E.-S., Tiirola, M., Nykänen, H., Martikainen, P.J., Yrjälä, K., Tuomivirta, T., and Fritze, H.: The role of Sphagnum mosses in the methane cycling of a boreal mire. Ecology, 91, 2356-2365, 2010.

Lindsay, R.: Mires. In: Finlayson C., Milton G., Prentice R., Davidson N. (eds) The Wetland Book. Springer, Dordrecht. https://doi.org/10.1007/978-94-007-4001-3_273, 2018.

Martin, M.: Cutadapt removes adapter sequences from high-throughput sequencing reads. 2011, 17, 3, 2011.

McCalley, C.K., Woodcroft, B.J., Hodgkins, S.B., Wehr, R.A., Kim, E.-H., Mondav, R., Crill, P.M., Chanton, J.P., Rich, V.I., Tyson, G.W., and Saleska, S.R.: Methane dynamics regulated by microbial community response to permafrost thaw. Nature, 514, 478-481, 2014.

McMurdie, P.J., and Holmes, S.: phyloseq: An R Package for Reproducible Interactive Analysis and Graphics of Microbiome Census Data. PLOS ONE, 8, e61217, 2013.

Menoud, M., van der Veen, C., Lowry, D., Fernandez, J. M., Bakkaloglu, S., France, J. L., Fisher, R. E., Maazallahi, H., Stanisavljević, M., Nęcki, J., Vinkovic, K., Łakomiec, P., Rinne, J., Korbeń, P., Schmidt, M., Defratyka, S., Yver-Kwok, C., Andersen, T., Chen, H., and Röckmann, T.: Global inventory of the stable isotopic composition of methane surface emissions, augmented by new measurements in Europe, Earth Syst. Sci. Data Discuss. [preprint], https://doi.org/10.5194/essd-2022-30, in review, 2022.

Meyer, F., Paarmann, D., D'Souza, M., Olson, R., Glass, E.M., Kubal, M., Paczian, T., Rodriguez, A., Stevens, R., Wilke, A., Wilkening, J., and Edwards, R.A.: The metagenomics RAST server – a public resource for the automatic phylogenetic and functional analysis of metagenomes. BMC Bioinformatics, 9, 386, 2008.

Mikaloff Fletcher, S.E., Tans, P.P., Bruhwiler, L.M., Miller, J.B., and Heimann, M.: CH4 sources estimated from atmospheric observations of CH4 and its 13C/12C isotopic ratios: 1. Inverse modeling of source processes. Global Biogeochem. Cy. 18:GB4004, doi:10.1029/2004GB002223, 2004a.

Mikaloff Fletcher, S.E., Tans, P.P., Bruhwiler, L.M., Miller, J.B., and Heimann, M.: CH4 sources estimated from atmospheric observations of CH4 and its 13C/12C isotopic ratios: 2. Inverse modeling of CH4 fluxes from geographical regions. Global Biogeochem. Cy. 18:GB4005, doi:10.1029/2004GB002224, 2004b.

Miller, J.B.: The carbon isotopic composition of atmospheric methane and its constraint on the global methane budget. In Flanagan, L.B., J.R. Ehleringer and D.E. Pataki (Eds.): Stable Isotopes and Biosphere-Atmosphere Interactions: Processes and Biological Controls. Elsevier, pp. 288-310, 2005.

Mondav, R., McCalley, C.K., Hodgkins, S.B., Frolking, S., Saleska, S.R., Rich, V.I., Chanton, J.P., and Crill P.M.: Microbial network, phylogenetic diversity and community membership in the active layer across a permafrost thaw gradient. Environmental Microbiology, 19, 3201-3218, https://doi.org/10.1111/1462-2920.13809, 2017.

Monteil, G., Houweling, S., Dlugockenky, E.J., Maenhout, G., Vaughn, B.H., White, J.W.C., and Rockmann, T.: Interpreting methane variations in the past two decades using measurements of CH4 mixing ratio and isotopic composition, Atmos. Chem. Phys., 11, 9141–9153, 2011.

O'Leary, N.A., Wright, M.W., Brister, J.R., Ciufo, S., Haddad, D., McVeigh, R., Rajput, B., Robbertse, B., Smith-White, B., Ako-Adjei, D., Astashyn, A., Badretdin, A., Bao, Y., Blinkova, O., Brover, V., Chetvernin, V., Choi, J., Cox, E., Ermolaeva, O., Farrell, C.M., Goldfarb, T., Gupta, T., Haft, D., Hatcher, E., Hlavina, W., Joardar, V.S., Kodali, V.K., Li, W., Maglott, D., Masterson, P., McGarvey, K.M., Murphy, M.R., O'Neill, K., Pujar, S., Rangwala, S.H., Rausch, D., Riddick, L.D., Schoch, C., Shkeda, A., Storz, S.S., Sun, H., Thibaud-Nissen, F., Tolstoy, I., Tully, R.E., Vatsan, A.R., Wallin, C., Webb, D., Wu, W., Landrum, M.J., Kimchi, A., Tatusova, T., Dicuccio, M., Kitts, P., Murphy, T. D., and Pruitt, K.D.: Reference sequence (RefSeq) database at NCBI: current status, taxonomic expansion, and functional annotation. Nucleic Acids Res, 44, D733-45, 2016.

Oksanen, J., Blanchet, F.G., Friendly, M., Kindt, R., Legendre, P., McGlinn, D., Minchin, P.R., O'Hara, R.B., Simpson, G.L., Solymos, P., Henry, M., Stevens, H., Szoecs, E., and Wagner, H.: vegan: Community Ecology Package. 2019.

Penning, H., Plugge, C.M., Galand, P.E., and Conrad, R.: Variation of carbon isotope fractionation in hydrogenotrophic methanogenic microbial cultures and environmental samples at different energy status. Global Change Biology, 11, 2103–2113, doi: 10.1111/j.1365-2486.2005.01076.x, 2005.

R Core Team: R: A language and environment for statistical computing. Viena, Austria: R-Foundation for Statistical Computing, 2018.

Rinne, J., Riutta, T., Pihlatie, M., Aurela, M., Haapanala, S., Tuovinen, J.-P., Tuittila, E.-S., and Vesala, T.: Annual cycle of methane emission from a boreal fen measured by the eddy covariance technique. Tellus, 59B, 449-457, 2007.

Rinne, J., Tuittila, E.-S., Peltola, O., Li, X., Raivonen, M., Alekseychik, P., Haapanala, S., Pihlatie, M., Aurela, M., Mammarella, I., and Vesala, T.: Temporal variation of ecosystem scale methane emission from a boreal fen in relation to temperature, water table position, and carbon dioxide fluxes. Global Biogeochemical Cycles, 32, 1087-1106, 2018.

Rinne, J., Tuovinen, J.-P., Klemedtsson, L., Aurela, M., Holst, J., Lohila, A., Weslien, P., Vestin, P., Łakomiec, P., Peichl, M., Tuittila, E.-S., Heiskanen, L., Laurila, T., Li, X., Alekseychik, P., Mammarella, I., Ström, L., Crill, P., and Nilsson, M.B.: Effect of the 2018 European drought on methane and carbon dioxide exchange of northern mire ecosystems. Philosophical Transactions of the Royal Society – B, 375, 20190517, 2020.

Rinne J., Ammann, C., Pattey, E., Paw U, K.T., and Desjardins, R.L.: Alternative Turbulent Trace Gas Flux Measurement Methods. In: Foken T. (eds) Springer Handbook of Atmospheric Measurements. Springer Handbooks. Springer, Cham. https://doi.org/10.1007/978-3-030-52171-4_56. pp. 1505-1530, 2021.

Riutta, T., Laine, J., Aurela, M., Rinne, J., Vesala, T., Laurila, T., Haapanala, S., Pihlatie, M., and Tuittila, E.-S.: Spatial variation in plant communities and their function regulates carbon gas dynamics in boreal fen ecosystem. Tellus, 59B, 838-852, 2007.

Röckmann, T., Eyer, S., van der Veen, C., Popa, M. E., Tuzson, B., Monteil, G., Houweling, S., Harris, E., Brunner, D., Fischer, H., Zazzeri,G., Lowry, D., Nisbet, E. G., Brand, W. A., Necki, J. M., Emmenegger, L., and Mohn, J.: In Situ Observations of the Isotopic Composition of Methane at the Cabauw Tall Tower Site, Atmospheric Chemistry and Physics, 16, 10 469–10 487, https://doi.org/10.5194/acp-16-10469-5752016, 2016.

Serrano-Silva, N., Sarria-Guzmán, Y., Lendooven, L., and Luna-Guido, M.: Methanogenesis and methanotrophy in Soil: A review. Pedosphere, 24, 291-307, 2014.

Sriskantharajah, S., Fisher, R.E., Lowry, D., Aalto, T., Hatakka, J., Aurela, M., Laurila, T., Lohila, A., Kuitunen, E., and Nisbet, E.G.: Stable carbon isotope signatures of methane from a Finnish subarctic wetland. Tellus B, 64, 18818, http://dx.doi.org/10.3402/tellusb.v64i0.18818, 2012

Villanueva, R.A.M., and Chen, Z.J.: ggplot2: Elegant Graphics for Data Analysis (2nd ed.). Measurement: Interdisciplinary Research and Perspectives, 17, 160-167, 2019.

White, J. D., Ström, L., Lehsten, V., Rinne, J., and Ahrén, D.: Genetic functional potential displays minor importance in explaining spatial variability of methane fluxes within a Eriophorum vaginatum dominated Swedish peatland, Biogeosciences Discuss. [preprint], https://doi.org/10.5194/bg-2021-353, in review, 2022.

Tables

Table 1 : Dominant vegetation in flux chambers. D : dominant ; P : present. Niche indicates the niche of the species. The relative elevation (above 80 m a.s.l.) of moss surface at each chamber is indicated.

SPECIES	**CH_1 13 CM**	**CH_2 6 CM**	**CH_3 6 CM**	**CH_4 14 CM**	**CH_5 20 CM**	**CH_6 3 CM**	**NICHE**
Rhynchospora alba	D	D	-	-	-	D	Wet
Eriophorum vaginatum	-	-	P	$D^{50\%}$	P	P	Wet - Moist
Andromeda polifolia	-	-	P	-	-	-	Moist
Myrica gale	-	-	-	$D^{50\%}$	D	P	Moist
Erica tetralix	-	-	P	P	P	P	Moist
Calluna vulgaris	-	-	P	P	-	-	Moist – Dry
Sphagnum papillosum	-	-	D	P	-	-	Moist

Table 2 : Proportions of different vegetation types in different radii around the NBLA tower.

Radius [m]	Wet hollows [%]	Dry hummocks [%]	Trees [%]
20	20	78	1.0
50	16	76	7.2
100	17	75	8.6

Table 3 : Results of SIMPER analysis between intermediate (n = 7) and wet (n = 4) plots. Functional group are ranked according to their average contribution to dissimilarity between plots. Standard deviation (SD), average abundances, percentage of cumulative contribution and permutation *p*-value (Probability of getting a larger or equal average contribution in random permutation of the group factor) are also included.

Functional group	Average dissimilarity	SD	Average abundance intermediate	Average abundance Wet	Cumulative Percentage	p
Hydrogenotrophic methanogens	0.30	0.19	3155	20214	48%	0.10
Type II methanotrophs	0.18	0.13	3583	11503	76%	0.08
Hydr/Methyl/Aceto methanogens	0.06	0.03	839	3844	85%	0.13
Type I methanotrophs	0.05	0.04	821	3006	93%	**0.01**
Verrucomicrobia	0.03	0.02	281	1482	97%	**0.00**
Methylotrophic methanogens	0.01	0.01	94	715	99%	**0.03**
Acetoclastic methanogen	0.01	0.01	80	605	100%	0.13

Table 4 : Results of SIMPER analysis between intermediate (n = 7) and dry (n = 6) plots. Taxa are ranked according to their average contribution to dissimilarity between plots. Standard deviation (SD), average abundances, percentage of cumulative contribution and permutation *p*-value (Probability of getting a larger or equal average contribution in random permutation of the group factor) are also included.

Functional Group	Average dissimilarity	SD	Average abundance intermediate	Average abundance dry	Cumulative Percentage	p
Hydrogenotrophic methanogens	0.21	0.16	3155	4050	52%	0.95
Type II methanotrophs	0.11	0.10	3583	2105	80%	0.96
Hydr/Methyl/Aceto.methanogens	0.05	0.04	839	1100	92%	0.77
Type I methanotrophs	0.02	0.01	821	676	97%	0.99
Acetoclastic methanogens	0.01	0.01	80	104	98%	0.91
Methylotrophic methanogens	0.00	0.00	94	110	99%	0.97
Verrucomicrobia	0.00	0.00	281	294	100%	1.00

Table 5 : Results of SIMPER analysis between wet (n = 4) and dry (n = 6) plots. Taxa are ranked according to their average contribution to dissimilarity between plots. Standard deviation (SD), average abundances, percentage of cumulative contribution and permutation *p*-value (Probability of getting a larger or equal average contribution in random permutation of the group factor) are also included.

Functional Group	Average dissimilarity	SD	Average abundance wet	Average abundance dry	Cummulative Percentage	p
Hydrogenotrophic methanogens	0.30	0.18	20214	4050	47.46%	0.11
Type II methanotrophs	0.19	0.12	11503	2105	77.08%	**0.04**
Hydr/Methyl/Aceto methanogens	0.05	0.03	3844	1100	85.58%	0.39
Type I methanotrophs	0.05	0.04	3006	676	93.15%	**0.00**
Verrucomicrobia	0.03	0.02	1482	294	97.20%	**0.00**
Methylotrophic methanogens	0.01	0.01	715	110	98.70%	**0.05**
Acetoclastic methanogens	0.01	0.01	605	104	100.00%	0.14